Journal of Quality Measurement and Analysis
e-ISSN: 2600-8602
https://doi.org/10.17576/jqma.2103.2025.11

JQMA 21(3) 2025, 175-189
http://www.ukm.my/jqma

THE FLOW AND THERMAL PROPERTIES OF RADIATING MAGNETOHYDRODYNAMICS HYBRID NANOFLUID OVER AN INCLINED PLANE

(*Sifat-sifat Aliran dan Terma Magnetohidrodinamik Nanobendalir Hibrid Memancar di atas Satah Condong*)

NANTHINI BALAKRISHNAN, SITI SUZILLIANA PUTRI BINTI MOHAMED ISA* & NURUL SYUHADA ISMAIL

ABSTRACT

In recent times, incorporating nanoparticles when studying the boundary layer flow has caught attention of many researchers due their promising abilities to elevate the thermal exchange within a fluid structure. In virtue of the vast applications in engineering and industrial fields, extending/compressing sheet, magnetic field and thermal radiation have been the persistently added controlling effects to the flow environment through years. Subsequently, this study investigates the flow and thermal properties of Ethylene Glycol (EG) magnetohydrodynamics hybrid nanofluid accommodating $CoFe_2O_4$ and TiO_2 nanoparticles passing a slanted extending/compressing plane with thermal radiation. Employing similarity transformation, the problem's governing equations are altered to an array of ordinary differential equations. The solver function for boundary value problem (bvp4c) provided by MATLAB software is applied to numerically solve these ordinary differential equations. The occurrence of numerical solutions for specific values of volume fraction of nanoparticles has been observed upon utilization of MATLAB. For diverse values of the parameter, the findings for flow and thermal profiles are portrayed graphically. Additionally, the influence of extending/compressing sheet rate and volume fraction of nanoparticles on the skin friction coefficient and local Nusselt number are also investigated. It has been perceived that the profiles of flow and thermal are enhanced when volume fraction of $CoFe_2O_4$ and TiO_2 are increased for the extending plane case. The opposite effects in flow and thermal profiles are noticed for compressing plane case.

Keywords: hybrid nanofluid; thermal radiation; extending/compressing inclined plane

ABSTRAK

Sejak kebelakangan ini, penggabungan nanozarah dalam kajian aliran lapisan sempadan menjadi perhatian ramai penyelidik kerana kebolehan zarah-zarah tersebut untuk meningkatkan prestasi pertukaran haba dalam sesebuah sistem bendalir. Disebabkan aplikasi dalam bidang kejuruteraan dan industri yang luas, satah memanjang/memampat, medan magnet dan pancaran haba menjadi elemen mengawal yang ditambah kepada persekitaran aliran secara berterusan selama ini. Seterusnya, kajian ini menyiasat sifat-sifat aliran dan terma magnetohidrodinamik nanobendalir hibrid etilena glikol (EG) dengan nanozarah-nanozarah $CoFe_2O_4$ dan TiO_2 di atas satah condong memanjang/memampat dengan pancaran haba. Menggunakan kaedah transformasi persamaan, persamaan yang mengawal ditransformasikan kepada set persamaan pembezaan biasa. Fungsi penyelesai bagi masalah nilai sempadan (bvp4c) dalam perisian MATLAB telah digunakan untuk menyelesaikan persamaan-persamaan pembezaan biasa tersebut secara berangka. Kewujudan penyelesaian berangka untuk nilai khusus pecahan isipadu nanozarah diperhatikan setelah menggunakan perisian MATLAB. Untuk pelbagai nilai parameter tersebut, penemuan bagi profil halaju dan terma dipersembahkan dalam bentuk graf. Tambahan pula, impak pecahan isipadu nanozarah dan kadar memanjang/memampat terhadap pekali geseran permukaan dan nombor Nusselt tempatan juga disiasat. Ia didapati bahawa profil halaju dan terma dipertingkatkan apabila pecahan isipadu $CoFe_2O_4$ dan TiO_2 ditingkatkan bagi kes satah memanjang. Kesan yang bertentangan terhadapa profil halaju dan terma dapat diperhatikan bagi kes satah memampat.

Kata kunci: nanobendalir hibrid; pancaran haba; satah condong memanjang/memampat

1. Introduction

Hybrid nanofluids are composite products of blending of duplet or additional diissimilar types of nano-sized particles into a base fluid. Cobalt ferrite ($CoFe_2O_4$) nanoparticles have gained noteworthy attention recently attributable to their special magnetic characteristics and promising applications in several fields, including biomedicine, catalysis, and environmental remediation. Besides, titanium dioxide (TiO_2) nanoparticles are widely studied and utilized in various fields due to their excellent photocatalytic, antibacterial, and ultraviolet (UV)-blocking properties. Ethylene glycol is a clear, odorless, and slightly viscous liquid with excellent thermal properties, making it suitable to be a base fluid for a nanofluid.

Magnetohydrodynamics (MHD) is the examination of electrically conducting fluids under the influence of magnetic field. The magnetic field contributes essential part in regulating the flow of thermal transfer in a system which can be useful in MHD generators, crystal growth and metal casting. In addition, thermal radiation refers to the emission of energy from a heated surface in the guise of electromagnetic radiation to all directions at the speed of light without any propagation medium. Gas-cooled reactors, nuclear power plants and hypersonic aircrafts use the concept of radiation. The benefits of magnetic field and radiation has motivated researchers to employ these effects when studying the dynamics of fluids. The Darcy-Forchheimer flow of TiO_2-Al_2O_3/H_2O induced by a rotating disk with velocity slip and nonlinear heat radiation are carried out by Thakur *et al.* (2023). The stagnation point stream of Al_2O_3-TiO_2-Cu/H_2O flowing through a compressing disk under the impact of magnetic field and heat radiation is presented by Yasir & Khan (2024). The unsteady flow of Casson fluid-based Ag-TiO_2 inside a rotating frame over a vertical moving surface with the exponential variation on the velocity, velocity slip, and magnetic field was investigated by Krishna *et al.* (2021). Raju *et al.* (2015) examined the influence of shape factor of nanoparticles and magnetic field on the mixed convective stream of Ag-TiO_2/H_2O through a slender cylinder. The effects of heat radiation, magnetic effects, and suction on the stagnation point stream of $CoFe_2O_4$-TiO_2/H_2O induced by a compressing cylinder was remarked by Waini *et al.* (2022b). The case of MHD stream of Ag-TiO_2/H_2O passing an elongating/compressing wedge under the impact of thermal radiation and viscous dissipation is considered by Kho *et al.* (2023). The heat production factor is added by Patil & Kulkarni (2021) to the MHD stream of Ag-TiO_2/H_2O passing an elongating/compressing sheet with heat radiation. Recently, the MHD flow of Fe_3O_4-$CoFe_2O_4$/kerosene oil through an exponentially shortening sheet positioned vertically with the factor of heat production/absorption and heat radiation is examined by Yusuf *et al.* (2020).

Stretching or shrinking sheet refers to an elastic sheet that is extended or compressed when stress is applied. Over decades, the boundary layer flow through a shortening/elongating sheet has hold a special importance among researchers due to advantages in cooling of stripes, paper production, production of rubber sheet (stretching sheet) and helicopter rotor, ship propeller (shrinking sheet). Ghadikolaei *et al.* (2017) examined the stagnation point stream of TiO_2-Cu/H_2O passing through a horizontally positioned elongating sheet with the influence of induced magnetic field. Similar hybrid nanofluid is used by Gholinia *et al.* (2018) to investigate the boundary layer flow through a lengthening surface with linear velocity. The consequences of employing thermal generation/absorption towards the stagnation point stream of polysterene-TiO_2/H_2O through an elongating sheet is considered by Masood *et al.* (2021). The time-dependent flow of Maxwell hybrid nanofluid (Al_2O_3-Cu/Sodium Algate) flowing through a stretching/shrinking sheet is explored by Zainal *et al.* (2021). Apart from sheet, stretching/shrinking Riga plate was considered by Zainal *et al.* (2022) to study the non-steady stagnation point flow of Al_2O_3-Cu/H_2O under the presence of thermal radiation. The boundary layer flow of $CoFe_2O_4$-(Mn-$ZnFe_2O_4$) ferrofluid induced by nonlinearly elongating flat sheet posi-

tioned in a porous medium is examined by Mansourian *et al.* (2022). The impacts of suction and heat radiation on the MHD stream of Fe_3O_4 induced by a biaxially elongating/shortening sheet is outlined by Khashi'ie *et al.* (2022). The heat sink/source factor is employed by Usafzai *et al.* (2022) on the unsteady flow of $CoFe_2O_4$-(Mn-$ZnFe_2O_4$)/H_2O flowing through a shrinking sheet. Usafzai *et al.* (2023) acquired exact solutions in the structure of exponential integral, Kummers function and Euler's gamma function for Cu-H_2O nanofluid flowing through a permeable extending/compressing sheet including the effects of temperature jump and velocity slip. Yahaya *et al.* (2024) considered four nanoparticles namely Al_2O_3, TiO_2, Cu and Ag to study the traditional Glauert wall jet flow with velocity slip, moving wall conditions, and wall mass transfer. Patel *et al.* (2023) considered the impacts of second order velocity slip and heat source on the free convective flow of Cu-Fe_2O_4/H_2O induced by an elongating sheet. Waini *et al.* (2019) appraised the influence of Newtonian heating, heat radiation and viscous dissipation when studying the MHD mixed convective stream of TiO_2-Al_2O_3-SiO_2/H_2O passing through a lengthening sheet with non-uniform thickness.

The prime intention of current study is to extend preceding research done by Waini *et al.* (2022a). They studied the passing of Cu-Al_2O_3/H_2O through a lengthening/shortening sheet. This study targets to occupy the gap in the work done by Waini *et al.* (2022a) by adding the effect of inclination factor, incorporating magnetic effects, using $CoFe_2O_4$-TiO_2/Ethylene Glycol as hybrid nanofluid instead of Cu-Al_2O_3/H_2O and considering both stretching and shrinking case for the inclined sheet. The novelty of present study is to clearly report the impacts of volume fraction of nanoparticles on the associated profiles and physical parameters for opposing flow case.

2. Mathematical Formulation

The submergence of dual nanoparticles, $CoFe_2O_4$ and TiO_2 in ethylene glycol is considered for current paper as Figure 1 portrays.

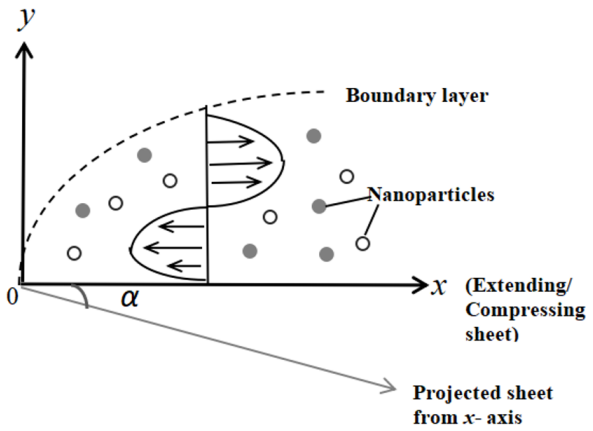

Figure 1: Illustration of current flow model

The extending/compressing plane which is originally located at the horizontal axis, is projected by a certain amount of angle, α. The velocity of this plane is indicated by u_w, together with it's rate of extension/compression, λ. However, the horizontal (x- axis) and vertical (y-axis) components of the hybrid nanofluid's velocity are recognized with u and v. The compression case, the extending case and the static case for the plane are determined by the values of $\lambda < 0$, $\lambda > 0$, and $\lambda = 0$, respectively. The fluid movement is affected by the gravitational acceleration, g and magnetic field, B. For the initial formulation, the symbols of nanoparticles are not introduced yet due to the assumption that the mixture (nanoparticles + base fluid) is sta-

ble. Following Waini *et al.* (2022a) and adding the inclination factor alongside magnetic field effects, the governing equations are as follows,

$$\frac{\partial u}{\partial x}+\frac{\partial v}{\partial y}=0, \tag{1}$$

$$u\frac{\partial u}{\partial x}+v\frac{\partial u}{\partial y}=\frac{\mu_{hnf}}{\rho_{hnf}}\frac{\partial^2 u}{\partial y}+g\beta_T(T-T_\infty)\cos\alpha-\frac{\sigma_{hnf}B^2}{\rho_{hnf}}u, \tag{2}$$

$$u\frac{\partial T}{\partial x}+v\frac{\partial T}{\partial y}=\frac{k_{hnf}}{(\rho C_p)_{hnf}}\frac{\partial^2 T}{\partial y^2}-\frac{1}{(\rho C_p)_{hnf}}\frac{\partial q_r}{\partial y}, \tag{3}$$

where μ_{hnf}, ρ_{hnf}, σ_{hnf}, k_{hnf}, $(\rho C_p)_{hnf}$ refers to the dynamic viscosity, density, electrical conductivity, thermal conductivity and the heat capacitance of the hybrid nanofluid, β_T is the coefficient of thermal expansion, T is the hybrid nanofluid's temperature, subscript ∞ refers to the value far away from the plane and q_r is the radiation flux. For the energy equation (Eq. (3)), the final derivation inclusive of thermal radiation effect with the usage of Rosseland approximation (Saeed *et al.* 2021) has been described in the previous paper by Waini *et al.* (2022a). Therefore, this paper follows the final derivation of the energy equation by Waini *et al.* (2022a) as shown in Eq. (4).

$$u\frac{\partial T}{\partial x}+v\frac{\partial T}{\partial y}=\left[\frac{k_{hnf}}{(\rho C_p)_{hnf}}+\frac{16\sigma^* T_\infty^3}{3(\rho C_p)_{hnf}K^*}\right]\frac{\partial^2 T}{\partial y^2}, \tag{4}$$

where σ^* and K^* refers to the Stefan-Boltzmann constant and coefficient of mean absorption respectively. The Rosseland approximation is used due to the assumptions in the fluid model such as the nanofluid is optically thick, which means that the fluid is highly absorbing and scattering so that radiation is locally in equilibrium. The second assumption is the nanofluid must has low temperature gradients, by this trend: If the temperature changes gradually, the approximation holds. Finally, the nanofluid will has a diffusion-dominated regime, means that the radiation is treated similarly to heat conduction. The velocity of fluid is little caused by a laminar flow, thus viscous thermal dissipation is anticipated to be slightest. The effective thermophysical attributes for nanofluid and hybrid nanofluid are displayed in Table 1. The subscripts hnf, nf, f and s refer to the hybrid nanofluid, nanofluid, base fluid and the nanoparticle respectively. Meanwhile, Table 2 presents the values for thermophysical attributes of nanoparticles ($CoFe_2O_4$ and TiO_2) and the base fluid (Ethylene Glycol). The boundary conditions are as follows,

$$\begin{aligned} &v=v_w(x), \quad u=u_w(x)\lambda, \quad T=T_w, \quad \text{at} \quad y=0,\\ &u\to 0, \quad T\to T_\infty, \quad \text{as} \quad y\to\infty. \end{aligned} \tag{5}$$

The succeeding similarity variables are applied to reduce the above-mentioned governing equations as depicted by Waini *et al.* (2022a),

$$\begin{aligned} &u=\frac{v_f}{L^{\frac{4}{3}}}x^{\frac{1}{3}}f'(\eta), \quad v=-\frac{1}{3}\frac{v_f}{L^{\frac{2}{3}}}x^{-\frac{1}{3}}[2f(\eta)-\eta f'(\eta)],\\ &B(x)=B_0\nu_f^{1/2}x^{-1/3}L^{-2/3}, \quad \theta(\eta)=\frac{T-T_\infty}{T_w-T_\infty}, \quad \eta=y\frac{x^{-\frac{1}{3}}}{L^{\frac{2}{3}}}, \end{aligned} \tag{6}$$

where η represents the similarity variable for boundary layer thickness and L is the characteristic length of the inclined plane. The previous investigators have showed the following:

$$u_w(x)=\left(\frac{v_f}{L^{\frac{4}{3}}}\right)x^{\frac{1}{3}}, \quad v_w=-\frac{1}{3}\frac{\nu_f}{L^{\frac{2}{3}}}x^{-\frac{1}{3}}[2f(\eta)-\eta f'(\eta)]S, \tag{7}$$

Table 1: The thermophysical attributes of nanofluid and hybrid nanofluid

Properties	Nanofluid
Density	$\rho_{nf} = (1-\phi_1)\rho_f + \phi_1\rho_{s1}$
Heat capacity	$(\rho C_p)_{nf} = (1-\phi_1)(\rho C_p)_f + \phi_1(\rho C_p)_{s1}$
Dynamic viscosity	$\mu_{nf} = \frac{\mu_f}{(1-\phi_1)^{2.5}}$
Electrical conductivity	$\sigma_{nf} = \frac{\sigma_{s1}+2\sigma_f-2\phi_1(\sigma_f-\sigma_{s1})}{\sigma_{s1}+2\sigma_f+\phi_1(\sigma_f-\sigma_{s1})} \times \sigma_f$
Thermal conductivity	$k_{nf} = \frac{k_{s1}+2k_f-2\phi_1(k_f-k_{s1})}{k_{s1}+2k_f+\phi_1(k_f-k_{s1})} \times k_f$
Properties	**Hybrid Nanofluid**
Density	$\rho_{hnf} = (1-\phi_2)\left[(1-\phi_1)_{\rho_f} + \phi_1\rho_{s1}\right] + \phi_2\rho_{s2}$
Heat capacity	$(\rho C_p)_{nf} = (1-\phi_2)\left[(1-\phi_1)(\rho C_p)_f + \phi_1(\rho C_p)_{s1}\right]$ $+\phi_2(\rho C_p)_{s2}$
Dynamic viscosity	$\mu_{hnf} = \frac{\mu_f}{(1-\phi_1)^{2.5}(1-\phi_2)^{2.5}}$
Electrical conductivity	$\sigma_{hnf} = \frac{\sigma_{s2}+2\sigma_{nf}-2\phi_2(\sigma_{nf}-\sigma_{s2})}{\sigma_{s2}+2\sigma_{nf}+\phi_2(\sigma_{nf}-\sigma_{s2})} \times \sigma_{nf}$
Thermal conductivity	$k_{hnf} = \frac{k_{s2}+2k_{nf}-2\phi_2(k_{nf}-k_{s2})}{k_{s2}+2k_{nf}+\phi_2(k_{nf}-k_{s2})} \times k_{nf}$

Table 2: Thermo-physical properties of Ethylene Glycol (Ramzan *et al.* 2020; Zainal *et al.* 2021), Cobalt Ferrite (Waini *et al.* 2022b), and Titanium Dioxide (Waini *et al.* 2022b)

	$\rho\,(kg/m^3)$	$C_p\,(J/kgK)$	$k(W/mK)$	$\sigma(S/m)$	Pr
Ethylene Glycol (EG)	1115	2430	0.253	1.07×10^{-4}	204
$CoFe_2O_4$	4907	700	3.7	5.51×10^{9}	-
TiO_2	4250	686.2	8.9538	2.38×10^{6}	-

where S is the steady mass flux parameter, with $S > 0$ denoting suction and $S < 0$ denoting injection.

In our study, inserting Eqs. (6) and (7) into Eqs. (1), (2) and (4) gives the following equations,

$$\frac{\mu_{\frac{hnf}{\mu_f}}}{\rho_{\frac{hnf}{\rho_f}}} 3f''' - f'^2 + 2ff'' + \varepsilon\theta cos\alpha - 3\frac{\sigma_{hnf}}{\sigma_f}Mf' = 0, \tag{8}$$

$$\frac{3}{Pr}\frac{\frac{k_{hnf}}{\kappa_f}}{\frac{(\rho C_p)_{hnf}}{(\rho C_p)_f}}\left[1+\frac{4}{3\frac{k_{hnf}}{\kappa_f}}Rd\right]\theta'' + 2f\theta' = 0, \tag{9}$$

where $Rd = 4\sigma^* T_\infty^3/K^* k_f$ refers to the radiation parameter, $Pr = \mu_f(C_p)_f/k_f$ refers to the Prandtl number, $\varepsilon = \frac{3L^{\frac{8}{3}}x^{\frac{1}{3}}}{\nu_f^2} g\beta_T(T_w - T_\infty)$ is the mixed convection parameter, and $M = \frac{\sigma_f B_0^2}{\rho_f}$ is the parameter of magnetic field. The primes in Eqs. (8)-(10) denote the function differentiation with respect to η. The boundary conditions from Eq. (5) are transformed as given,

$$\begin{aligned} &f(0) = S, \quad f'(0) = \lambda, \quad \theta(0) = 1, \\ &f'(\infty) \to 0, \quad \theta'(\infty) \to 0. \end{aligned} \tag{10}$$

The skin friction coefficient, C_f and the local Nusselt number, Nu_x are the physical param-

eters of ultimate attention in practical implementations, defined as,

$$C_f = \frac{\tau_w}{\rho_f u_w^2}, \quad Nu_x = \frac{xq_w}{k_f(T_w - T_\infty)}, \tag{11}$$

with,

$$\tau_w = \mu_{hnf}\left(\frac{\partial u}{\partial y}\right)_{y=0}, \quad q_w = -k_{hnf}\left(\frac{\partial T}{\partial y}\right)_{y=0} + (q_r)_{y=0}\,, \tag{12}$$

where τ_w denotes the shear stress along the plane and q_w denotes the heat flux from the plane. The skin friction coefficient and Nusselt number can be transformed as follows by substituting Eqs. (6), (7) and (12) into (11) to get,

$$C_f Re_x^{\frac{1}{2}} = \frac{\mu_{hnf}}{\mu_f} f''(0), \quad Nu_x Re_x^{\frac{1}{2}} = -\left(\frac{k_{hnf}}{k_f} + \frac{4}{3}Rd\right)\theta'(0), \tag{13}$$

where $Re_x = u_w(x)x/\nu_f$ is called the local Reynold's number.

3. Results & Discussion

Eqs. (8) and (9) has been analysed using the method of bvp4c MATLAB programming with the boundary conditions as expressed in Eq. (10). This study implements $CoFe_2O_4$ (first nanoparticle) and TiO_2 (second nanoparticle) dispersed in Ethylene Glycol (EG). The present study identifies some fixed parameters unless otherwise stated: Prandtl number, $Pr = 204$ (based fluid Ethylene Glycol), volume fraction of nanoparticle 1, $\phi_1 = 0.1$, volume fraction of nanoparticle 2, $\phi_2 = 0.6$, thermal radiation, $Rd = 0.5$, suction, $S = 4$, compressing sheet, $\lambda = -0.1$, extending sheet, $\lambda = 0.5$, inclined angle, $\alpha = 60^\circ$, and mixed convection parameter (opposing flow), $\epsilon = -0.5$. It is worth mentioning that the effects of influential parameters on the flow and thermal attributes of the hybrid nanofluid is similar for both opposing and assisting flow case. Thus, this paper only demonstrates the findings for the opposing flow case.

The outcome data are portrayed graphically for velocity profiles, $f'(\eta)$ and temperature profiles, $\theta(\eta)$ for diverse values ϕ_1 and ϕ_2 as presented in Figures 2-9, respectively. Moreover, resulting data for the skin friction coefficient, $C_f Re_x^{1/2}$ and local Nusselt number, $Nu_x Re_x^{1/2}$ are also depicted in Figures 10-13. The solid line in the graphical results represents the least value of the influential parameter, whereas the dotted line represents the highest value of the same parameter. Besides, the dashed line is the influential parameter's value which is in between the highest and the least values.

3.1. *Verification of current method*

By contrasting the current results with those from earlier investigations, as tabulated in Tables 3 and 4, the numerical solutions are validated. When radiation parameter, $Rd = 0$, mixed convection parameter, $\epsilon = 0$, inclination angle, $\alpha = 0$ and $\lambda = 1$ (extending sheet), for diverse values of S, Table 3 shows the numerical data of $f''(0)$ for regular fluid $(\phi_1 = \phi_2 = 0)$. It is remarked that the current outcomes are in great consent with the results perceived by Cortell (2014), Ferdows *et al.* (2013) and Rosseland (1931). The values of $-\theta'(0)$ for regular fluid $(\phi_1 = \phi_2 = 0)$ when radiation parameter, $Rd = 0$, mixed convection parameter, $\epsilon = 0$, inclination angle, $\alpha = 0$, $\lambda = 1$ (stretched sheet) and the Prandtl number, $Pr = 2$ for different values of S and Rd are tabulated in Table 4. The current data for $-\theta'(0)$ coincides greatly with the results acquired by Cortell (2014), Ferdows *et al.* (2013) and Rashidi *et al.* (2014). It could be pointed out from Table 3 and 4 that the current numerical scheme used to solve the flow

model is valid.

Table 3: The numerical values of $f''(0)$ for regular fluid ($\phi_1 = \phi_2 = 0$) when $R = \epsilon = \alpha = 0$ and $\lambda = 1$

S	Cortell (2014)	Ferdows *et al.* (2013)	Rosseland (1931)	Waini *et al.* (2022a)	Present results
0.75	-0.984417	-0.984439	-0.9844401	-0.984439	-0.984439
0.5	-0.873627	-0.873643	-0.8736447	-0.873643	-0.873643
0	-0.677647	-0.677648	-0.6776563	-0.677648	-0.677648
-0.5	-0.518869	-0.518869	-0.5188901	-0.518869	-0.518869
-0.75	-0.453521	-0.453523	-0.4535499	-0.453523	-0.453523
-0.8	-	-	-	-	-0.441533
-0.9	-	-	-	-	-0.418592

Table 4: The numerical values of $-\theta'(0)$ for regular fluid ($\phi_1 = \phi_2 = 0$) when $R = \epsilon = \alpha = 0$ and $\lambda = 1$

S	R	Cortell (2014)	Ferdows *et al.* (2013)	Rosseland (1931)	Rashidi *et al.* (2014)	Waini *et al.* (2022a)	Present results
-0.5	1	0.2873620	0.287483	0.2877091	0.2877091	0.287485	0.287485
	0	0.3989462	0.398951	0.3990842	0.3990842	0.399100	0.399099
0	1	0.4430879	0.443323	0.4434039	0.443404	0443323	0.443323
	0	0.7643554	0.764374	0.7643525	0.7643527	0.764357	0.764357
0.5	1	0.6322154	0.632199	0.6322186	0.6322187	0.632200	0.632200
	0	1.2307661	1.230952	1.2307912	1.2307916	1.230792	1.230792
0.7	1	-	-	-	-	-	0.715512
	0	-	-	-	-	-	1.438099

3.2. *Extending sheet case*

For extending sheet case, $\lambda = 0.5$, Figures 2-3 show the numerical illustration on the trend of $f'(\eta)$ and $\theta(\eta)$ when the various ϕ_1 values which is 0.1, 0.2 and 0.3 are applied. As we can see in Figure 2, the rise of $f'(\eta)$ are caused by the growth of ϕ_1. Figure 3 displays that increasing ϕ_1 can cause an increment in the temperature profile. Reasoning behind both results is that as the volume fraction of nanoparticle increases, a significant increase in the thermal conductivity occurs. This thermal elevation eventually thickens the boundary layer and lastly takes on the rise in velocity function (Al-Sankoor *et al.* 2021). Therefore, more heat will be absorbed by the fluid resulting in a higher temperature.

When different values of ϕ_2 such as 0.06, 0.2 and 0.3 are used, the effects of $f'(\eta)$ and $\theta(\eta)$ are shown in Figures 4-5. From Figure 4, it is noticeable that as the value of ϕ_2 getting higher, $f'(\eta)$ inclines. Similarly, Figure 5 displays that the increase of $\theta(\eta)$, are reasoned by the increase of ϕ_2. Therefore, the higher the value of ϕ_2, the greater the radiant thermal energy being pumped into the fluid stream increasing the temperature.

3.3. *Compressing sheet case*

For compressing sheet case, $\lambda = -1.0$, Figures 6-7 exhibit the velocity profiles, $f'(\eta)$ and temperature profiles, $\theta(\eta)$ for various values of ϕ_1 which is $\phi_1 = 0.1, 0.2, 0.3$. The obtained results in Figure 6 show that when ϕ_1 is increased, $f'(\eta)$ decreases. Figure 7 shows that a rise in ϕ_1 causes an incline in $\theta(\eta)$. Based on both figures, it is obvious that when the volume fraction

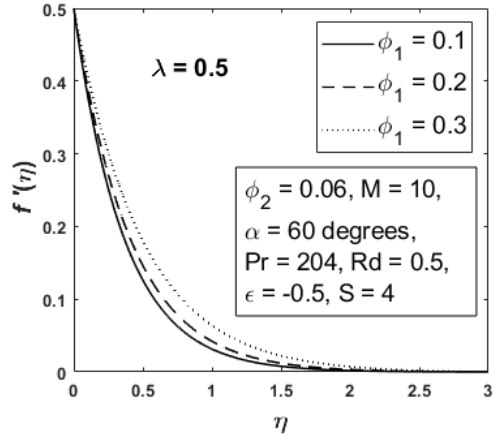

Figure 2: The impact of different values of ϕ_1 on $f'(\eta)$ for $\lambda = 0.5$

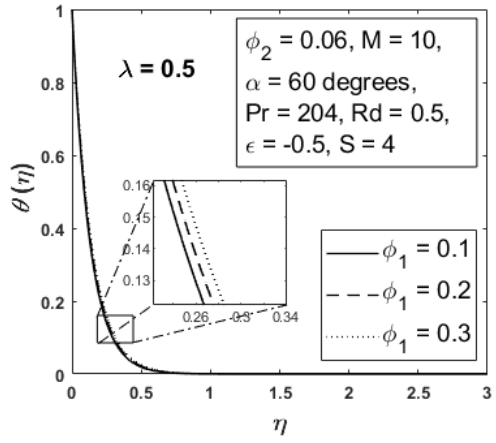

Figure 3: The impact of different values of ϕ_1 on $\theta(\eta)$ for $\lambda = 0.5$

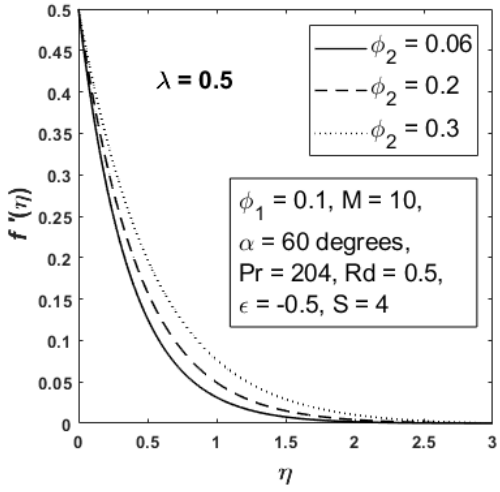

Figure 4: The impact of different values of ϕ_2 on $f'(\eta)$ for $\lambda = 0.5$

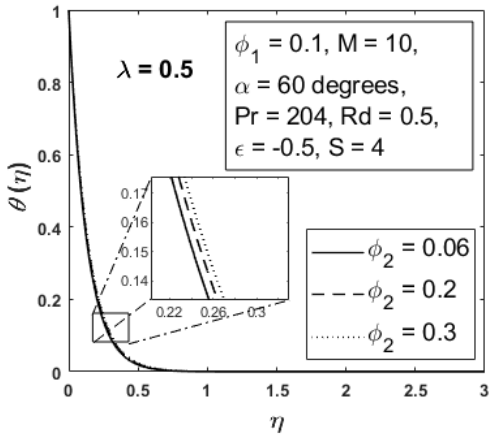

Figure 5: The impact of different values of ϕ_2 on $\theta(\eta)$ for $\lambda = 0.5$

of nanoparticle rises, the fluid's velocity drops meanwhile the temperature profile enhances. From Figure 8, it can be observed that the $f'(\eta)$ is lessened due to the rise of ϕ_2. Meanwhile, Figure 9 shows that the higher the value of ϕ_2, the higher the $\theta(\eta)$. Abbas & Magdy (2020) stated that it happens because the density of the nanofluid lessened with a rise in the volume fraction of nanoparticles, improving thermal conductivity and speeding up the rate of surface heat exchange whilst thickening the thermal boundary layer.

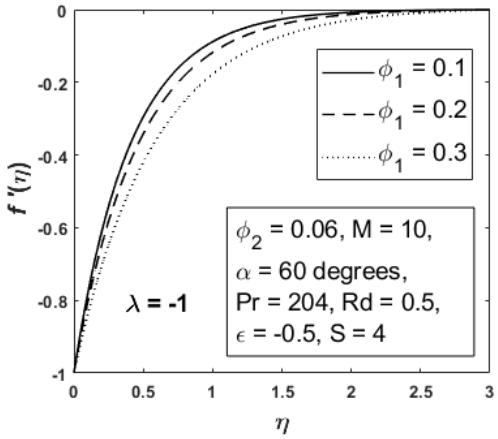

Figure 6: The impact of different values of ϕ_1 on $f'(\eta)$ for $\lambda = -1.0$

3.4. *Skin friction coefficient and local Nusselt number*

The graphical results of skin friction coefficient, $C_f Re_x^{1/2}$ and local Nusselt number, $Nu_x Re_x^{1/2}$ from Eq. (13) are illustrated in Figures 10-11 for both extending and compressing plane cases when various values of ϕ_1 are applied. From Figures 10-11, it could be seen that the range of λ for $\phi_1 = 0.1$ is $-1.69167 \leq \lambda \leq 0.76460$, for $\phi_1 = 0.4$ is $-1.72089 \leq \lambda \leq 0.78967$, and lastly for $\phi_1 = 0.5$ is $-1.15192 \leq \lambda \leq 0.75221$. The widest λ range is produced by $\phi_1 = 0.4$, whereas the smallest range of λ is owned by $\phi_1 = 0.5$. The increment of ϕ_1 causes the decrement of $C_f Re_x^{1/2}$ for negative λ values (compressing case), whereas induces an enhancement of $C_f Re_x^{1/2}$ for positive λ values (extending case). Meanwhile, the local Nusselt

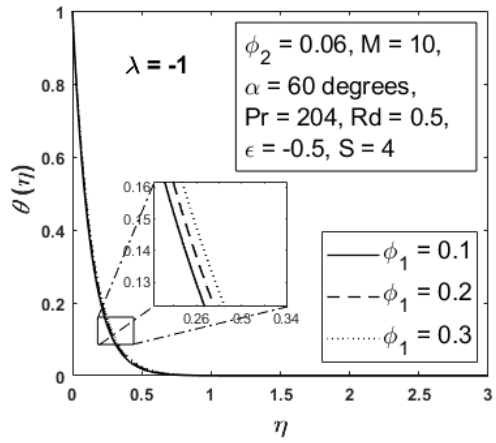

Figure 7: The impact of different values of ϕ_1 on $\theta(\eta)$ for $\lambda = -1.0$

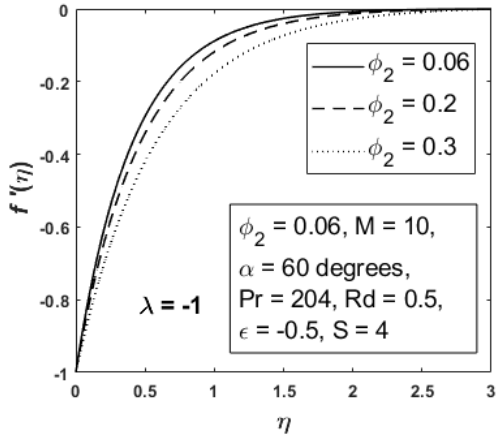

Figure 8: The impact of different values of ϕ_2 on $f'(\eta)$ for $\lambda = -1.0$

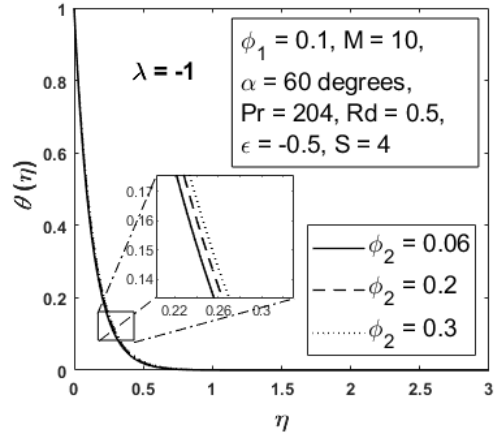

Figure 9: The impact of different values of ϕ_2 on $\theta(\eta)$ for $\lambda = -1.0$

number declines for both cases when the values of ϕ_1 is increased.

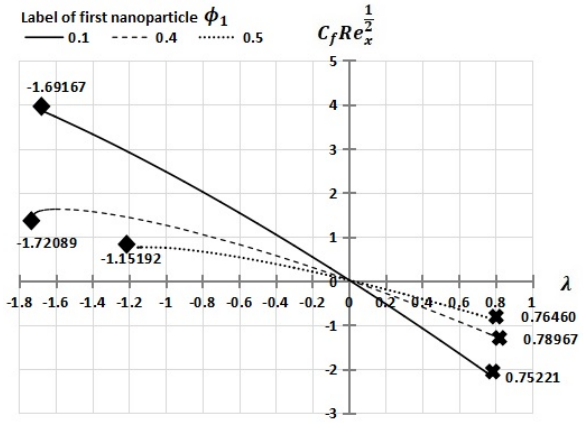

Figure 10: The graph of $C_f Re_x^{\frac{1}{2}}$ against λ for diverse values of ϕ_1

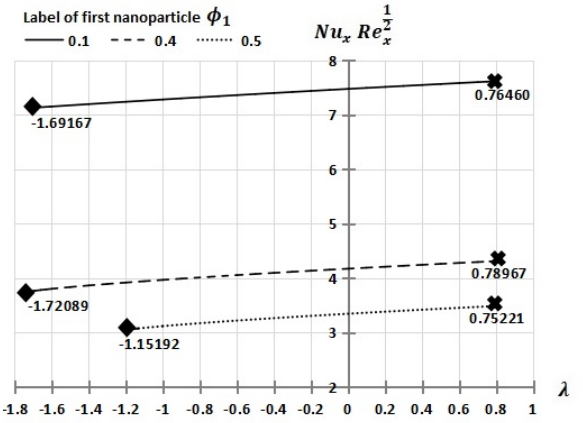

Figure 11: The graph of $Nu_x Re_x^{\frac{1}{2}}$ against λ for diverse values of ϕ_1

When different values of ϕ_2 are applied, the graphical results of local skin friction coefficient, $C_f Re_x^{\frac{1}{2}}$ and the local Nusselt number, $Nu_x Re_x^{\frac{1}{2}}$ for both extending and compressing surface cases are presented in Figures 12-13. Grounded from our computation, it is noticeable that the range of λ for $\phi_2 = 0.06$ is $-1.69167 \leq \lambda \leq 0.76460$, for $\phi_2 = 0.2$ is $-1.70000 \leq \lambda \leq 0.77969$, and lastly for $\phi_2 = 0.3$ is $-1.88576 \leq \lambda \leq 0.79159$. The widest λ range is owned by $\phi_2 = 0.3$, whereas the lowest range of λ is given by $\phi_2 = 0.06$. The trend of $C_f Re_x^{1/2}$ and $Nu_x Re_x^{1/2}$ for different values of ϕ_2 is similar to that of ϕ_1 for both positive and negative λ values.

4. Conclusions

Ethylene glycol is a polar, organic liquid with the specific properties that make it ideal as a base fluid for nanofluids. It has high boiling point (197°C), which is suitable for high-temperature applications. Besides, it has low freezing point, which is appropriate to use as antifreeze and coolants. Ethylene glycol has good thermal stability and suits in harsh environments. Finally,

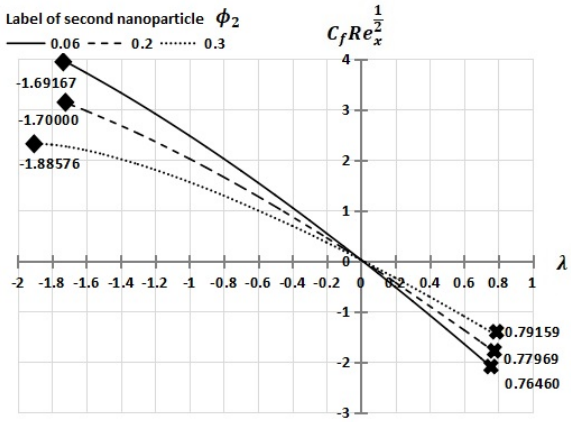

Figure 12: The graph of $C_f Re_x^{\frac{1}{2}}$ against λ for diverse values of ϕ_2

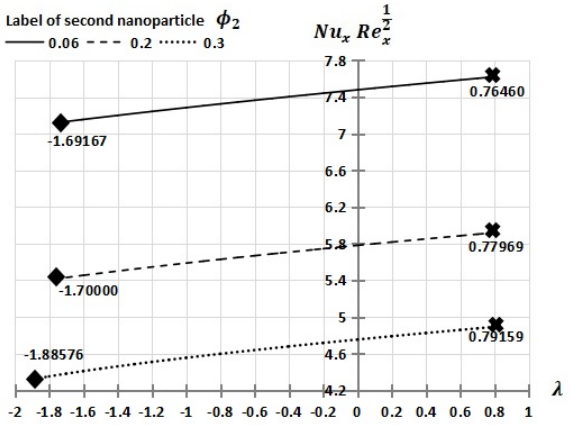

Figure 13: The graph of $Nu_x Re_x^{\frac{1}{2}}$ against λ for diverse values of ϕ_2

it has low volatility, which means that it has minimum risk in evaporation losses. Cobalt ferrite has high electrical resistivity, excellent magnetic properties, and good chemical stability. $CoFe_2O_4$-based nanofluids are widely used in magnetothermal applications, heat transfer enhancement, biomedical fields, and industrial cooling systems due to their ability to respond to external magnetic fields while improving thermal conductivity. Meanwhile, titanium dioxide is a widely used nanoparticle in nanofluids due to its high thermal conductivity, chemical stability, non-toxicity, and photocatalytic properties. TiO_2-based nanofluids are extensively applied in heat transfer, solar energy, biomedical, lubrication, and environmental applications. The concentration of the dual nanoparticles affecting the velocity and temperature of the hybrid nanofluid, with Ethylene Glycol acting as a base fluid is investigated through mathematical model, and solved by numerical approach. The similarity parameters are used to obtain the nonlinear differential equations. These equations are numerically resolved utilizing the bvp4c built-in function in MATLAB software. The velocity, temperature alongside the skin friction coefficient and local Nusselt number were determined and reviewed in detail. The important discoveries of current study are listed as following:

(1) It is clear from the verification of results that MATLAB programming is suitable for obtaining numerical solutions.
(2) In stretching cases, the increment of the volume fraction of nanoparticles causes the rising

of the velocity component that will also make the thermal properties to rise. This applied to both the nanoparticles.

(3) While in shrinking case, the velocity component decreases with the increase of nanoparticle's volume fraction. In contrast, thermal attributes incline with the rise in nanoparticle's volume fraction. It held true for both the nanoparticles.
(4) The increment in volume fraction of $CoFe_2O_4$ and TiO_2 decreases the skin friction coefficient for compressing plane case.
(5) The increment in volume fraction of $CoFe_2O_4$ and TiO_2 increases the skin friction coefficient for extending plane case.
(6) The inclination in the volume fraction of both $CoFe_2O_4$ and TiO_2 reduces the local Nusselt number for both the extending and compressing plane cases.

Acknowledgement

This research was funded by a grant from Universiti Putra Malaysia (Project code: GP-IPS/2023 /9782800).

References

Abbas W. & Magdy M.M. 2020. Heat and mass transfer analysis of nanofluid flow based on Cu, Al_2O_3, and TiO_2 over a moving rotating plate and impact of various nanoparticle shapes. *Mathematical Problems in Engineering* **2020**: 9606382.

Al-Sankoor K., Al-Gayyim H., Al-Musaedi S., Asadi Z. & Ganji D.D. 2021. Analytically investigating of heat transfer parameters with presence of graphene oxide nanoparticles in Williamson-magnetic fluid by AGM and HPM methods. *Case Studies in Thermal Engineering* **27**: 101236.

Cortell R. 2014. Fluid flow and radiative nonlinear heat transfer over a stretching sheet. *Journal of King Saud University-Science* **26**(2): 161–167.

Ferdows M., Uddin M.J. & Afify A.A. 2013. Scaling group transformation for MHD boundary layer free convective heat and mass transfer flow past a convectively heated nonlinear radiating stretching sheet. *International Journal of Heat and Mass Transfer* **56**(1–2): 181–187.

Ghadikolaei S.S., Yassari M., Sadeghi H., Hosseinzadeh K. & Ganji D.D. 2017. Investigation on thermophysical properties of TiO_2–Cu/H_2O hybrid nanofluid transport dependent on shape factor in MHD stagnation point flow. *Powder Technology* **322**: 428–438.

Gholinia M., Gholinia S., Hosseinzadeh K. & Ganji D.D. 2018. Investigation on ethylene glycol nano fluid flow over a vertical permeable circular cylinder under effect of magnetic field. *Results in Physics* **9**: 1525–1533.

Khashi'ie N.S., Waini I., Wahid N.S., Arifin N.M. & Pop I. 2022. Radiative hybrid ferrofluid flow over a permeable shrinking sheet in a three-dimensional system. *CFD Letters* **14**(11): 9–21.

Kho Y.B., Jusoh R., Salleh M.Z., Ariff M.H. & Zainuddin N. 2023. Magnetohydrodynamics flow of Ag-TiO_2 hybrid nanofluid over a permeable wedge with thermal radiation and viscous dissipation. *Journal of Magnetism and Magnetic Materials* **565**: 170284.

Krishna M.V., Ahammad N.A. & Chamkha A.J. 2021. Radiative MHD flow of Casson hybrid nanofluid over an infinite exponentially accelerated vertical porous surface. *Case Studies in Thermal Engineering* **27**: 101229.

Mansourian M., Dinarvand S. & Pop I. 2022. Aqua cobalt ferrite/Mn–Zn ferrite hybrid nanofluid flow over a nonlinearly stretching permeable sheet in a porous medium. *Journal of Nanofluids* **11**: 383–391.

Masood S., Farooq M. & Anjum A. 2021. Influence of heat generation/absorption and stagnation point on polystyrene–TiO_2/H_2O hybrid nanofluid flow. *Scientific Reports* **11**: 22381.

Patel V.K., Pandya J.U. & Patel M.R. 2023. Testing the influence of TiO_2- Ag/water on hybrid nanofluid MHD flow with effect of radiation and slip conditions over exponentially stretching & shrinking sheets. *Journal of Magnetism and Magnetic Materials* **572**: 170591.

Patil P.M. & Kulkarni M. 2021. Analysis of MHD mixed convection in a Ag-TiO_2 hybrid nanofluid flow past a slender cylinder. *Chinese Journal of Physics* **73**: 406–419.

Raju C.S.K., Sandeep N., Sulochana C., Sugunamma V. & Babu M.J. 2015. Radiation, inclined magnetic field and cross-diffusion effects on flow over a stretching surface. *Journal of the Nigerian Mathematical Society* **34**(2): 169–180.

Ramzan M., Gul N., Chung J.D., Kadry S. & Chu Y.M. 2020. Numerical treatment of radiative nickel–zinc ferrite-ethylene glycol nanofuid flow past a curved surface with thermal stratifcation and slip conditions. *Scientific Reports* **10**: 16832.

Rashidi M.M., Rostami B., Freidoonimehr N. & Abbasbandy S. 2014. Free convective heat and mass transfer for MHD fluid flow over a permeable vertical stretching sheet in the presence of the radiation and buoyancy effects. *Ain Shams Engineering Journal* **5**(13): 901–912.

Rosseland S. 1931. *Astrophysik: Auf Atomtheoretischer Grundlage*. Berlin, Germany: Springer Verlag.

Saeed A., Jawad M., Alghamdi W., Nasir S., Gul T. & Kumam P. 2021. Hybrid nanofluid flow through a spinning Darcy–Forchheimer porous space with thermal radiation. *Scientific Reports* **11**: 16708.

Thakur A., Sood S. & Sharma D. 2023. Mixed convective flow of tri-hybrid nanofluid TiO_2–Al_2O_3–SiO_2/H_2O past a variably thicked stretching sheet with Newtonian heating. *Journal of Nanofluids* **12**(7): 1782–1793.

Usafzai W.K., Aly E.H., Alshomrani A.S. & Ullah M.Z. 2022. Multiple solutions for nanofluids flow and heat transfer in porous medium with velocity slip and temperature jump. *International Communications in Heat and Mass Transfer* **131**: 105831.

Usafzai W.K., Haq R.U. & Aly E.H. 2023. Wall laminar nanofluid jet flow and heat transfer. *International Journal of Numerical Methods for Heat & Fluid Flow* **33**(5): 1818–1836.

Waini I., Ishak A. & Pop I. 2019. Hybrid nanofluid flow and heat transfer over a nonlinear permeable stretching/shrinking surface. *International Journal of Numerical Methods for Heat & Fluid Flow* **29**(9): 3110–3127.

Waini I., Khan U., Zaib A., Ishak A. & Pop I. 2022a. Inspection of TiO_2-$CoFe_2O_4$ nanoparticles on MHD flow toward a shrinking cylinder with radiative heat transfer. *Journal of Molecular Liquids* **361**: 119615.

Waini I., Khan U., Zaib A., Ishak A., Pop I. & Akkurt N. 2022b. Time-dependent flow of water-based $CoFe_2O_4$-$Mn-ZnFe_2O_4$ nanoparticles over a shrinking sheet with mass transfer effect in porous media. *Nanomaterials* **12**(22): 4102.

Yahaya R.I., Mustafa M.S., Md. Arifin N., Md. Ali F. & Mohamed Isa S.S.P. 2024. Response surface methodology on MHD stagnation-point flow of ternary hybrid nanofluid over a permeable radially shrinking disk. *Numerical Heat Transfer, Part A: Applications* **86**(13): 4324–4352.

Yasir M. & Khan M. 2024. Thermal efficiencies of Ohmic cobalt ferrite and magnetite hybrid ferrofluid flow over an exponentially vertically shrinking surface. *Alexandria Engineering Journal* **90**: 120–128.

Yusuf T.A., Mabood F., Khan W.A. & Gbadeyan J.A. 2020. Irreversibility analysis of Cu-TiO_2-H_2O hybrid-nanofluid impinging on a 3-D stretching sheet in a porous medium with nonlinear radiation: Darcy-Forchhiemer's model. *Alexandria Engineering Journal* **59**(6): 5247–5261.

Zainal N.A., Nazar R., Naganthran K. & Pop I. 2021. Unsteady flow of a Maxwell hybrid nanofluid past a stretching/shrinking surface with thermal radiation effect. *Applied Mathematics and Mechanics* **42**(10): 1511–1524.

Zainal N.A., Nazar R., Naganthran K. & Pop I. 2022. Unsteady stagnation point flow past a permeable stretching/shrinking Riga plate in $Al_2O_3 - Cu/H_2O$ hybrid nanofluid with thermal radiation. *International Journal of Numerical Methods for Heat & Fluid Flow* **32**(8): 2640–2658.

Institute for Mathematical Research,
Univerisiti Putra Malaysia,
43400, UPM Serdang,
Selangor, MALAYSIA
*E-mail: nanthinibalakrishnan53@gmail.com, ctsuzilliana@upm.edu.my**

Centre for Foundation Studies in Science of Universiti Putra Malaysia,
Universiti Putra Malaysia,
43400, UPM Serdang,
Selangor, MALAYSIA
*E-mail: ctsuzilliana@upm.edu.my**

Centre for Pre-University Studies,
Universiti Malaysia Sarawak,
94300 Kota Samarahan,
Sarawak, MALAYSIA
E-mail: insyuhada@unimas.my

Received: 7 August 2024
Accepted: 2 May 2025

*Corresponding author